Multi-component vapor-liquid equilibrium model for LES and application to ECN Spray A

Matheis, J; Hickel, Stefan

Important note
To cite this publication, please use the final published version (if applicable).
Please check the document version above.

Multi-component vapor-liquid equilibrium model for LES and application to ECN Spray A

By J. Matheis† AND S. Hickel‡

We present and evaluate a detailed multi-species two-phase thermodynamic equilibrium model for large-eddy simulations (LES) of liquid-fuel injection and mixing at high pressure. The model can represent the coexistence of supercritical states and multi-component subcritical two-phase states. LES results for the transcritical Spray A of the Engine Combustion Network (ECN) are found to agree very well with available experimental data. We also address well-known numerical challenges of trans- and supercritical fluid mixing and compare a fully conservative formulation to a quasi-conservative formulation of the governing equations. Our results prove physical and numerical consistency of both methods on fine grids and demonstrate the effects of energy-conservation errors associated with the quasi-conservative formulation on typical LES grids.

1. Introduction

We discuss large-eddy simulation (LES) results for the high-pressure liquid-fuel injection Spray A benchmark case of the Engine Combustion Network (ECN, `http://www.sandia.gov/ecn/`), with particular emphasis on both the physical and numerical modeling of the turbulent mixing of supercritical and transcritical fluids. The setup consists of a cold n-dodecane jet ($C_{12}H_{26}$ at 363 K) that is injected with about 600 m/s into a warm nitrogen (N_2) atmosphere at $T = 900$ K and a pressure of $p = 6$ MPa. This high pressure exceeds the critical pressure p_c of both components and results in a liquid-like ($p > p_c$, $T < T_c$) and a gas-like ($T > T_c$, $p > p_c$) state of the two pure species. However, the critical pressure of certain mixtures of the two species is much higher than the critical pressure of the pure species and also higher than the Spray A operating pressure, such that the mixture locally becomes subcritical and interfaces between liquid and gas phases may appear during the mixing process. We refer to such conditions as transcritical operating conditions. Previous numerical simulations of the transcritical Spray A have either modeled the spray with Lagrangian particle tracking (LPT) methods (see, e.g., Wehrfritz *et al.* 2013; Xue *et al.* 2013), i.e., as a classical two-phase spray with sharp gas-liquid interfaces (first- and secondary breakup, evaporative droplets), or with a single-phase dense-gas approach (see, e.g., Lacaze *et al.* 2015), arguing that the high pressure and temperature lead to a miscible mixing with negligible surface tension. Both approaches can be justified but have obvious limitations when applied to transcritical operating conditions that correspond to a transition regime between classical spray dynamics and miscible mixing. Standard LPT methods are very efficient computationally, but they neglect real-gas effects and dissolved ambient gases in the liquid fuel phase, which become substantial at high pressures (Balaji *et al.* 2011; Qiu & Reitz 2015). Furthermore, results can strongly depend on the values of calibration parameters. The single-phase dense-gas approach,

† Technical University of Munich, Germany
‡ Delft University of Technology, The Netherlands

on the other hand, does not include the effect of phase separation and may thus lead to unphysical or ill-defined states if part of the flow is subcritical. To improve on these limitations, and inspired by the work of Qiu & Reitz (2015), we have developed a detailed multi-species two-phase thermodynamic model for the Eulerian LES of turbulent mixing at supercritical and transcritical pressures, which can represent the coexistence of multi-component subcritical two-phase states in a computational cell.

2. Physical and numerical models

2.1. *Governing equations*

We solve the three-dimensional compressible multi-component Navier-Stokes equations either in a fully conservative (FC) formulation,

$$\partial_t \rho + \boldsymbol{\nabla} \cdot (\rho \mathbf{u}) = 0 \tag{2.1}$$

$$\partial_t \rho Y_i + \boldsymbol{\nabla} \cdot (\rho Y_i \mathbf{u}) = \boldsymbol{\nabla} \cdot \mathbf{J}_i \tag{2.2}$$

$$\partial_t \rho \mathbf{u} + \boldsymbol{\nabla} \cdot (\rho \mathbf{u}\mathbf{u} + \mathbf{I}p) = \boldsymbol{\nabla} \cdot \boldsymbol{\tau} \tag{2.3}$$

$$\partial_t E + \boldsymbol{\nabla} \cdot [(E + p)\mathbf{u}] = \boldsymbol{\nabla} \cdot (\mathbf{u} \cdot \boldsymbol{\tau} - \mathbf{q}) \ , \tag{2.4}$$

or in a quasi-conservative (QC) formulation for which the total energy conservation, Eq. (2.4), is replaced by the pressure evolution equation (see Terashima & Koshi 2012)

$$\partial_t p + \boldsymbol{\nabla} \cdot (p\mathbf{u}) = (p - \rho c^2)\boldsymbol{\nabla} \cdot \mathbf{u} + \frac{\alpha_p}{c_v \beta_T \rho} \left[\boldsymbol{\nabla} \cdot (\boldsymbol{\tau} \cdot \mathbf{u} - \mathbf{q}) - \mathbf{u} \cdot (\boldsymbol{\nabla} \cdot \boldsymbol{\tau}) \right] \dots$$
$$+ \sum_{i=1}^{N} \frac{1}{\rho} \frac{\partial p}{\partial Y_i}\bigg|_{\rho,e,Y_j[i]} \boldsymbol{\nabla} \cdot \mathbf{J}_i \ . \tag{2.5}$$

The state vector consists of mass density ρ, partial densities ρY_i of species $i = \{1 \dots N_c\}$, linear momentum $\rho \mathbf{u}$, and total energy density $E = \rho e + \frac{1}{2}\rho \mathbf{u} \cdot \mathbf{u}$ (FC) or the pressure p (QC). $\mathbf{u} = [u_1, u_2, u_3]^T$ is the velocity vector in a Cartesian frame of reference, c denotes the speed of sound, c_v is the heat capacity at constant volume, and α_p and β_T are the thermal expansion and isothermal compressibility coefficient. To allow for a meaningful comparison between FC and QC simulations we also included the effect of the diffusion-induced pressure variation, the last term on the right-hand side of Eq. (2.5), which was neglected by Terashima & Koshi (2012).

According to the Stokes hypothesis for a Newtonian fluid, the viscous stress tensor is $\boldsymbol{\tau} = \mu \left(\boldsymbol{\nabla}\mathbf{u} + (\boldsymbol{\nabla}\mathbf{u})^T - 2/3\,\mathbf{I}\,\boldsymbol{\nabla} \cdot \mathbf{u} \right)$, with μ being the dynamic viscosity and $\mathbf{I}$ the unit tensor. The diffusional fluxes are calculated via Fick's law $\mathbf{J}_i = \rho D_i \boldsymbol{\nabla} Y_i - Y_i \sum_{j=1}^{N} \rho D_j \boldsymbol{\nabla} Y_j$, where $D_i = (1 - z_i) / \sum_{j \neq i}^{N} z_j D_{ij}^{-1}$ is an effective binary diffusion coefficient for the diffusion of species i into the rest of the mixture and z_i denotes the mole fraction of species i. The physical binary mass diffusion coefficients D_{ij} are modeled according to Chapman and Enskog theory (see, e.g., Prausnitz *et al.* 1998). The vector $\mathbf{q} = -\kappa \boldsymbol{\nabla} T - \sum_{i=1}^{N} h_i \mathbf{J}_i$ consists of heat conduction and the enthalpy flux by species diffusion, where κ is the thermal conductivity, T is the temperature, and h_i is the partial enthalpy of species i. Helpful details on the calculation of partial properties can be found in Masquelet (2013). Viscosity and thermal conductivity are modeled with correlations given by Chung *et al.* (1988). The FC and QC equations are closed by a thermodynamic model that relates pressure, temperature and density.

2.2. *Multi-component single-phase equation of state*

Our single- and two-phase models are based on cubic equations of states (EOS)

$$p(\underline{v}, T, \mathbf{z}) = \frac{\mathcal{R}T}{\underline{v} - b} - \frac{a\alpha}{\underline{v}^2 + u\,b\,\underline{v} + wb^2}, \tag{2.6}$$

where the pressure p is a function of the molar volume $\underline{v}$, temperature T and the molar composition $\mathbf{z} = \{z_1 \ldots z_{N_c}\}$. Here and in the following, all intensive thermodynamic properties are expressed as molar quantities, denoted by $\underline{\star}$. $\mathcal{R}$ is the universal gas constant.

In all subsequent simulations we use the Peng-Robinson (PR) EOS (Peng & Robinson 1976) for which $u = 2$ and $w = -1$. The function $\alpha = [1 + c_0(1 - \sqrt{T_r})]^2$ accounts for the polarity of a fluid and is a correlation of temperature T, critical temperature T_c and acentric factor ω via $c_0 = 0.37464 + 1.54226\omega - 0.2699\omega^2$. The parameter $a = 0.45724\left(\mathcal{R}^2 T_c^2 / p_c\right)$ represents attractive forces between molecules and the effective molecular volume is represented by $b = 0.0778\left(\mathcal{R}T_c / p_c\right)$.

We use conventional mixing rules to extend the PR EOS to a mixture composed of N_c components. The parameters required in the EOS are calculated from

$$a\alpha = \sum_i^{N_c} \sum_j^{N_c} z_i z_j a_{ij} \alpha_{ij} \quad \text{and} \quad b = \sum_i^{N_c} z_i b_i, \tag{2.7}$$

with z_i being the mole fraction of component i (overall or in the liquid/vapor phase). The coefficients a_{ij} and α_{ij} are calculated with combination rules given by Harstad *et al.* (1997). We calculate off-diagonal elements using the same expression as for the diagonals together with pseudo-critical parameters

$$T_{c,ij} = \sqrt{T_{c,i} T_{c,j}}(1 - \delta'_{ij}) , \quad p_{c,ij} = Z_{c,ij}(\mathcal{R}T_{c,ij} / v_{c,ij}) , \tag{2.8}$$

$$v_{c,ij} = \frac{1}{8}\left[v_{c,i}^{1/3} + v_{c,j}^{1/3}\right]^3 , \quad \omega_{ij} = 0.5\left(\omega_i + \omega_j\right) , \quad Z_{c,ij} = 0.5\left(Z_i + Z_j\right) . \tag{2.9}$$

The binary interaction parameter δ'_{ij} is set to zero for all simulations in this report.

In addition to the thermal EOS, expressions for caloric properties (e.g., internal energy $\underline{e}$, specific heats $\underline{c}_p$ and $\underline{c}_v$, etc.) that account for their pressure dependance are needed. The departure function formalism provides such expressions and only requires relationships provided by the EOS (see, e.g., Poling *et al.* 2000). The ideal reference state is evaluated using the 9-coefficient NASA polynomials (Goos *et al.* 2009).

The single-phase frozen temperature (T_F) is computed iteratively by minimizing the objective function $F^{FC} = (\underline{e}^\star - \underline{e}_F(T_F, \underline{\rho}^\star, \mathbf{z}^\star))/\underline{e}^\star$ or $F^{QC} = (\underline{\rho}^\star - \underline{\rho}_F(T_F, p^\star, \mathbf{z}^\star))/\underline{\rho}^\star$, with $\underline{e}^\star = \underline{e}_{LES}$ (FC), $p^\star = p_{LES}$ (QC), $\underline{\rho}^\star = \underline{\rho}_{LES}$ and $\mathbf{z}^\star = \mathbf{z}_{LES}$ being the molar internal energy, pressure, molar density and overall molar composition that come from the flow solver (after conversion to molar quantities). Once the temperature is available, all other thermodynamic properties (e.g., pressure for FC formulation) and derivatives (e.g., specific heats, speed of sound, partial properties) can be calculated in a straightforward manner. Note that the pressure and temperature resulting from this single-phase model may correspond to unstable thermodynamic states.

2.3. *Multi-component two-phase equilibrium model*

A mixture is considered stable at the current temperature and pressure if and only if the total Gibbs energy is at its global minimum (Michelsen & Mollerup 2007). Whether a split into two phases yields a decrease in the Gibbs energy is determined by the Tangent

Plane Distance (TPD) function (Michelsen 1982). For the present work, we followed the recommendation of Qiu *et al.* (2014) and implemented the BFGS-quasi-Newton algorithm (see Hoteit & Firoozabadi (2006) and references therein). If the result of the TPD test tells us that the single-phase mixture is stable, then we apply the cubic EOS in a straightforward manner. If it turns out that the mixture is unstable, which means that the fluid would prefer to exist as two phases separated by an interface, then we solve the so-called isochoric-isoenergetic flash problem. Note that this implies the assumption that the phase-transition timescale is small compared to the flow timescale.

Temperature and pressure are iterated until the sum (weighted by the phase fraction) of the liquid-phase and vapor-phase densities and internal energies within a computational cell corresponds to the overall internal energy and density that come from the flow solver. The corresponding objective function for the two-phase equilibrium model is

$$\mathbf{F} = \left\{ \frac{\underline{v}^\star - \underline{v}_{EQ}(T,p,\mathbf{z}^\star)}{\underline{v}^\star}, \frac{\underline{e}^\star - \underline{e}_{EQ}(T,p,\mathbf{z}^\star)}{\underline{e}^\star} \right\} , \qquad (2.10)$$

with $\underline{e}^\star = \underline{e}_{LES}$, $\underline{v}^\star = \underline{v}_{LES}$ and $\mathbf{z}^\star = \mathbf{z}_{LES}$ being the specific molar internal energy and volume and overall composition in the corresponding cell, respectively.

In the innermost iteration loop we solve an isothermal isobaric flash problem, i.e., we calculate the vapor-liquid phase equilibrium (VLE) at given temperature, pressure and overall composition. The necessary condition of thermodynamic equilibrium is that the fugacity f_i of each component i is the same in the liquid (subscript l) and vapor (subscript v) phase, i.e., $f_{i,v}(T,p,\mathbf{y}) = f_{i,l}(T,p,\mathbf{x})$. We denote liquid and vapor phase mole fractions by $\mathbf{x} = \{x_1 \dots x_{N_c}\}$ and $\mathbf{y} = \{y_1 \dots y_{N_c}\}$, respectively. The material balance for each component, $\psi_v y_i + (1 - \psi_v)x_i = z_i$, with ψ_v being the overall molar vapor fraction, and the requirement that mole fractions in the liquid and vapor phase must sum to unity, or equivalently $\sum_{i=1}^{N_c} y_i - x_i = 0$, yield $(2N_c + 1)$ equations, which are solved for the unknown compositions $\mathbf{x}$ and $\mathbf{y}$ of liquid and vapor, and the molar vapor fraction ψ_v. Equilibrium volume $\underline{v}_{EQ}$ and energy $\underline{e}_{EQ}$ are then obtained as

$$\underline{v}_{EQ}(T,p,\mathbf{z}^\star) = \psi_v \underline{v}_v + (1 - \psi_v)\underline{v}_l \quad \text{and} \quad \underline{e}_{EQ}(T,p,\mathbf{z}^\star) = \psi_v \underline{e}_v + (1 - \psi_v)\underline{e}_l . \quad (2.11)$$

Specific molar volumes $(\underline{v}_v(T,p,\mathbf{y}),\underline{v}_l(T,p,\mathbf{x}))$ and energies $(\underline{e}_v(T,p,\mathbf{y}),\underline{e}_l(T,p,\mathbf{x}))$ of the two phases are calculated with the EOS (Eq. 2.6) and the departure function formalism, respectively. For a comprehensive review and practical implementation guidelines, the interested reader is referred to the textbook of Michelsen & Mollerup (2007).

2.4. *Discretization method and turbulence model*

The governing equations of the FC formulation, Eqs. (2.1)-(2.4), are discretized by a conservative finite-volume scheme. Effects of unresolved subgrid scales (SGS) are modeled by the adaptive local deconvolution method (ALDM) of Hickel *et al.* (2014). In order to avoid spurious oscillations at sharp density gradients, we use the van Albada limiter for the reconstruction of mass and internal energy. The viscous flux is discretized with a 2nd-order central difference scheme, and a 3rd-order explicit Runge-Kutta scheme is used for time integration. The left-hand side of the pressure evolution equation for the QC method is discretized consistently with the internal energy transport, such that both discretizations are identical up to machine precision for a single-species perfect gas.
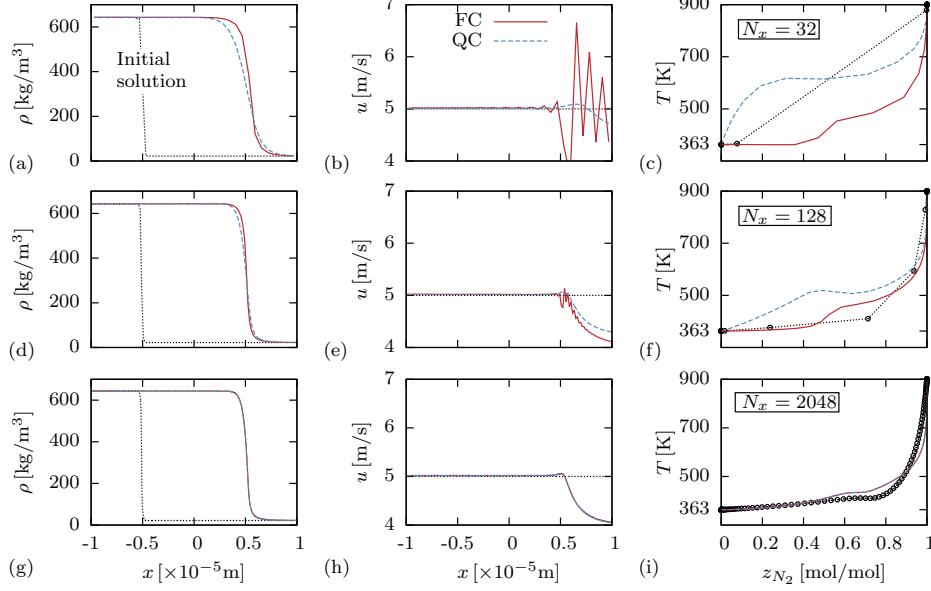
FIGURE 1. FC-F and QC-F results for a 1-D advection-diffusion test case for different grid resolutions. Left column: density profiles in physical space; center column: velocity profiles in physical space; right column: temperature profiles in mixture space; dotted lines are the initial profiles.

3. Interlude: consistency and convergence of FC and QC formulation

Equations (2.1)-(2.4), (2.1)-(2.3) and (2.5) are expected to converge to the same solution with increasing grid resolution. To prove this important hypothesis, we show results for a 1-D advection-diffusion test case of a contact discontinuity in Figure 1. The number of uniform cells in the region of interest $(-l_{ref}/2 < x < l_{ref}/2)$ with $l_{ref} = 2 \times 10^{-5}$ m varies from 32 to 2048. Two blocks with stretched cells are attached on both sides such that reflections from the boundary conditions cannot affect the results.

The chosen thermodynamic conditions are similar to Spray A ($p = 6$ MPa, $T_{N2} = 900$ K, $T_{C12H26} = 363$ K) and the advection velocity is $u = 5$ m/s. Species mass fractions are initialized with an error function profile in physical space

$$Y_{C12H26} = 0.5 - 0.5 \, \text{erf}\{(x_i + 0.25l_{ref})/(0.01l_{ref})\} \,, \tag{3.1}$$

with x_i being the cell-center coordinates. Both FC and QC equations are closed by the (frozen) single-phase model (FC-F and QC-F). The temperature across the initial interface is computed from a linear enthalpy profile in mixture space, commonly known as the adiabatic mixing temperature.

The first and second columns in Figure 1 show the density and velocity at $t = 2 \times 10^{-6}$s, and the dotted lines represent the initial solution at $t = 0$. The third column shows temperature profiles in mixture space, and point symbols along the dotted line visualize the number of grid points across the initial interface. We observe large differences between FC and QC formulations on the coarsest grid (Figure 1(a-c)). The FC method shows unphysical velocity oscillations, whereas the QC method yields smooth profiles. Note that physical diffusion causes a change in velocity on the right side of the advected contact discontinuity. The QC method shows much higher temperatures on the dodecane side (left) compared to the FC method. With increasing grid resolution, spurious oscillations
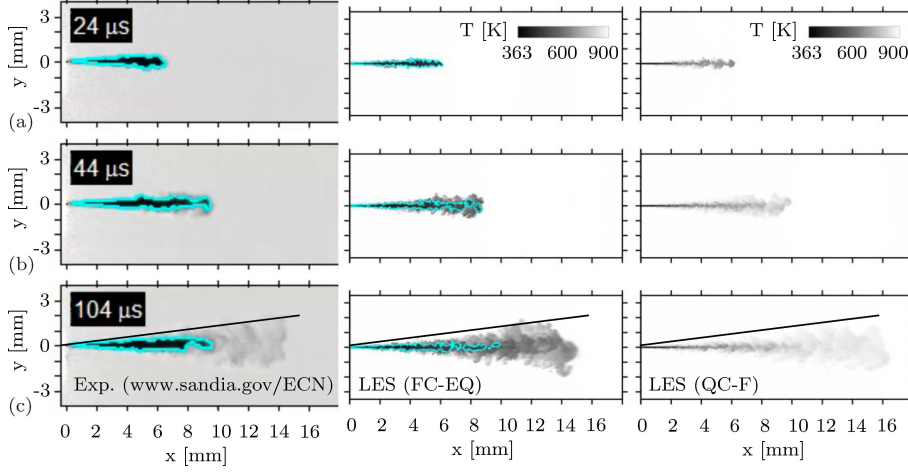
FIGURE 2. Temporal sequence of the injection event. Left column: experimental data of Pickett *et al.* (2011); center column: LES with FC-EQ; right column: LES with QC-F. Liquid penetration length is illustrated by a $LVF = 0.15\%$ isocontour.

of the FC method become less severe and eventually disappear, and the temperature profile of the QC method converges towards the FC solution. We conclude from these results that energy conservation errors – necessary to maintain velocity and pressure equilibria at interfaces without the generation of spurious oscillations – translate into errors in temperature on coarse grids and that both methods converge to the same solution on sufficiently fine grids. For typical LES grid resolutions, the energy conservation error of the QC method is non-negligible.

4. LES of ECN Spray A

All simulations have been performed in a rectangular domain with the overall dimensions $L_x = 56$ mm ($\sim 622D_i$) in the streamwise and $L_y = L_z = 28$ mm ($\sim 311D_i$) in the lateral directions. An adaptive Cartesian blocking strategy with a static local coarsening/refinement is used to allow for a varying grid resolution along the spray break-up trajectory to keep computational costs tractable. The grid consists of 2766 blocks with 7 grid refinement levels and a total number of about 15.1 million cells. A velocity block profile without turbulent fluctuations is prescribed at the inflow patch. The time-dependent mass flow rate is taken from `http://www.cmt.upv.es/ECN03.aspx` with the following input parameters: injection pressure: 150 MPa; outlet diameter: $D_i = 0.09$ mm; fuel density: 703.82 kg/m^3; back pressure: 6 MPa; discharge coefficient: 0.89; injection time: 1.5 ms. At the outlet we prescribe the static pressure of 6 MPa. All walls are adiabatic.

In the following we use experimental reference data to evaluate our numerical results obtained with the quasi-conservative frozen single-phase model (QC-F) and with the fully conservative equilibrium two-phase model (FC-EQ). The fully conservative single-phase method (FC-F) encountered numerical instabilities during the start-up phase when the jet accelerates from 0 to 600 m/s in just 10 μs. A total time interval of 1.5 ms has been simulated. Figure 2 depicts a temporal sequence of the early jet evolution (24μs-104μs). The left column shows experimental data (diffused back illumination). The center and right columns show snapshots of the temperature distribution for LES with FC-EQ and QC-F methods, respectively. In the case of FC-EQ, the liquid penetration length is illus-
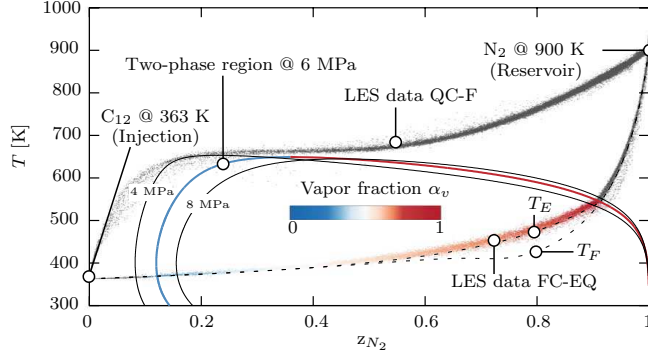
FIGURE 3. Temperature-composition diagram for a $N_2 - C_{12}H_{26}$ mixture with frozen (T_F) and equilibrium (T_E) mixing temperature. Scattered data depict the thermodynamic states that are obtained in the QC-F and FC-EQ LES at 144 μs. For FC-EQ, points within the two-phase region are colored by vapor volume fraction.

trated by the cyan iso-contour of the liquid volume fraction $LVF = 0.15\%$. We observe a very good qualitative agreement between experimental data and LES with the FC-EQ method. At 24 μs the liquid dodecane jet extends about 6mm into the nitrogen atmosphere, at about 44 μs the liquid length has reached its quasi-steady mean. Later points in time illustrate the vapor evolution. QC-F and FC-EQ simulations predict a very similar vapor penetration trajectory; however, significant differences are observed for the temperature field. The dense dodecane jet heats up more quickly and mixing takes place at much higher temperatures with the QC-F model. This effect is not caused by the thermodynamic modeling approach (assumed single-phase vs. two-phase), but rather by energy conservation errors of the QC method. Figure 3 shows a temperature-composition phase diagram for the nitrogen-dodecane mixture together with frozen (T_F) and equilibrium (T_E) mixing temperature. The two-phase region is indicated at a pressure of 6 MPa (nominal operating pressure), 4 MPa and 8 MPa. Scattered data depict the thermodynamic states that are obtained in the LES with the methods FC-EQ and QC-F, instantaneous data is taken from Figure 2(c). In the case of FC-EQ, data points within the two-phase region are colored by the vapor volume fraction from blue to red shades. While the FC-EQ LES follows closely the equilibrium mixing temperature, we observe a completely different mixing for the QC-F LES. We have previously shown that the QC-F temperature prediction will eventually converge towards FC solution within the single-phase region when increasing the number of cells, i.e., reducing the energy conservation error. We therefore conclude that, for the present application and typical LES grid resolutions, the energy conservation error of the QC method is not controllable.

A quantitative comparison between experiment and the FC-EQ LES is given in Figure 4(a) showing liquid and vapor penetration trajectories. In the LES, the liquid core length is defined as $L_l = \max\{x(LVF = 0.15\%)\}$, vapor penetration L_v is shown for the definitions $\max\{x(Y_{C12H26} = 1\%)\}$ and $\max\{x(Y_{C12H26} = 0.001\%)\}$. We observe an excellent agreement of L_l with the experimental time-resolved signal. Note that the measured L_l depends on the chosen threshold value. Based on a thorough analysis based on Mie-scatter theory together with assumptions on droplet diameters, Pickett *et al.* (2011) conclude that the LVF threshold representing their liquid length is expected to be less than 0.15% at Spray A conditions. The experimental time-averaged liquid length fluctuates by approximately ±1mm about the quasi-steady mean of 10.4mm; this value is in ex-

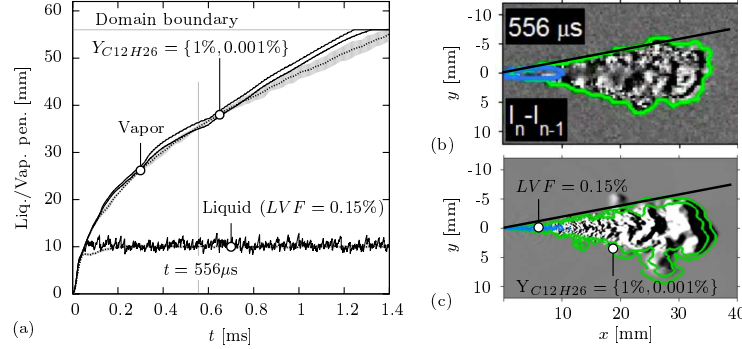FIGURE 4. (a) Numerical (———) and experimental (··········) liquid and vapor penetration trajectories. (b) Experimental schlieren image. (c) Numerical schlieren image for FC-EQ LES.
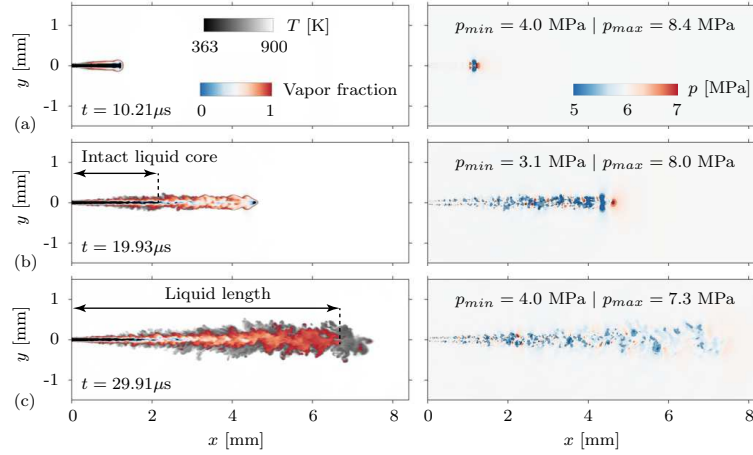

FIGURE 5. Temporal sequence of temperature (left) and pressure (right) for FC-EQ LES.

cellent agreement with our LES data for the threshold value of 0.15%. In order to evaluate the sensitivity on the threshold value we computed L_l for $LVF = \{3\%, 1\%, 0.15\%, 0.05\%\}$ and obtained $L_l = \{8.83, 9.91, 10.40, 10.49\}$mm, respectively.

We also observe a good agreement of the vapor penetration trajectory up to ~ 0.8ms. At later times the penetration depth is slightly overpredicted. In the experiment, the vapor penetration length is derived from high-speed schlieren images. Figure 4(b-c) gives an impression on how a mixture fraction threshold compares to a schlieren image. The numerical schlieren image shows the axial density gradient $\partial\rho/\partial x$ spatially averaged along the z-direction. Numerical and experimental images are strikingly similar. Quantitatively, a definition of the vapor penetration depth by a 1% mixture fraction threshold seems to slightly underpredict the vapor penetration derived from a schlieren image, mainly in the long-term evolution. We therefore do not recommend tracking values larger 1%.

Figure 5 shows a temporal sequence of the spray structure in the near-nozzle field at a very early state, 10 μs, 20 μs and 30 μs after the injection start. In the left column we show instantaneous snapshots of the temperature field (contour levels are shown for 363 K $< T <$ 900 K, dark to light gray shades). Superimposed is the vapor volume fraction distribution (blue to red shades) for the two-phase region within which the isochoric-isoenergetic flash problem was solved. Contours of the corresponding pressure

fields (5 MPa $< p <$ 7 MPa, from blue to red shades) are shown in the right column. We see that the dodecane-nitrogen mixture locally experiences pressures much different from the average ambient pressure. A very low pressure ($\sim$ 3 MPa) can be observed at the tip of the jet due to the start-up vortex ring. Even in the fully developed steady state, we see pressure fluctuations in the shear layer in the order of $\pm$10 bar.

We mentioned above that we were not able to simulate Spray A with a conservative single-phase model (FC-F). The instabilities encountered are caused by our single-phase thermodynamics, which yields ill-defined states at low pressures that occur in well resolved vortex cores. Our fully conservative two-phase LES model (FC-EQ) did not face any stability problems because the more sophisticated model can resolve coexisting subcritical two-phase states, thus avoiding unphysical states.

5. Conclusion

A detailed multi-species two-phase thermodynamic equilibrium model for the Eulerian LES of turbulent mixing at high pressures has been presented and applied for LES of liquid-fuel injection at transcritical operating conditions. The thermodynamics model is based on cubic equations of state and vapor-liquid equilibrium calculations. This model can thus accurately represent supercritical states as well as coexisting multi-component subcritical two-phase states. Computational results for the transcritical dodecane injection ECN Spray A case demonstrate the excellent performance of the model. We saw that the Spray A dodecane-nitrogen mixture locally experiences pressures significantly below the nominal operating pressure of 6 MPa when the jet accelerates from 0 to 600 m/s in just 10 μs. For these harsh conditions, LES with a conservative dense-gas single-phase approach exhibit large spurious pressure oscillations that may cause numerical instability even with low-order upwind numerics. It has been suggested previously that stable time integration of single-phase thermodynamic models can be obtained by energy-correction methods that sacrifice energy conservation in some way. We therefore compared a fully conservative formulation of the governing equations with a quasi-conservative formulation based on a pressure evolution equation. A one-dimensional multi-component advection-diffusion test cases proved physical and numerical consistency of both methods and convergence towards the same solution for sufficiently fine grids. On coarser grids, however, energy conservation errors associated with the quasi-conservative formulation caused a significant overprediction of the temperature. LES with our new fully conservative multi-component two-phase equilibrium model did not show any stability problems and yielded numerical predictions that are in very good agreement with available experimental data.

REFERENCES

BALAJI, B., RAGHAVAN, V., RAMAMURTHI, K. & GOGOS, G. 2011 A numerical study of evaporation characteristics of spherical n-dodecane droplets in high pressure nitrogen environment. *Phys. Fluids* **23**, 063601.

Chung, T. H., Ajlan, M., Lee, L. L. & Starling, K. E. 1988 Generalized multi-parameter correlation for nonpolar and polar fluid transport properties. *Ind. Eng. Chem. Res.* **27**, 671–679.

Goos, E., Burcat, A. & Ruscic, B. 2009 Third Millennium Ideal Gas and Condensed Phase Thermochemical Database for Combustion. *http://burcat.technion.ac.il/dir*.

Harstad, K., Miller, R. S. & Bellan, J. 1997 Efficient high-pressure state equations. *AIChE J.* **43**, 1605–1610.

Hickel, S., Egerer, C. P. & Larsson, J. 2014 Subgrid-scale modeling for implicit large eddy simulation of compressible flows and shock-turbulence interaction. *Phys. Fluids* **26**, 106101.

Hoteit, H. & Firoozabadi, A. 2006 Simple phase stability-testing algorithm in the reduction method. *AIChE J.* **52**, 2909–2920.

Lacaze, G., Misdariis, A., Ruiz, A. & Oefelein, J. C. 2015 Analysis of high-pressure Diesel fuel injection processes using LES with real-fluid thermodynamics and transport. *Proc. Combust. Inst.* **35**, 1603–1611.

Masquelet, M. M. 2013 *Large-eddy simulations of high-pressure shear coaxial flows relevant for H2/O2 rocket engines*. PhD thesis, Georgia Institute of Technology.

Michelsen, M. L. 1982 The isothermal flash problem. Part I. Stability. *Fluid Phase Equilibr.* **9**, 1–19.

Michelsen, M. L. & Mollerup, J. M. 2007 *Thermodynamic Models: Fundamentals & Computational Aspects*. Tie-Line Publications.

Peng, D. Y. & Robinson, D. B. 1976 A new two-constant equation of state. *Ind. Eng. Chem. Fund.* **15**, 59–64.

Pickett, L. M., Genzale, C. L., Manin, J., Malbec, L. M. & Hermant, L. 2011 Measurement uncertainty of liquid penetration in evaporating Diesel sprays. In *Proceedings of the 23rd Annual Conference on Liquid Atomization and Spray Systems*.

Poling, B., Prausnitz, J. & O' Connell, J. 2000 *The properties of gases and liquids*. McGraw Hill.

Prausnitz, J. M., Lichtenthaler, R. N. & de Azevedo, E. G. 1998 *Molecular Thermodynamics of Fluid-Phase Equilibria*. Pearson Education.

Qiu, L. & Reitz, R. D. 2015 An investigation of thermodynamic states during high-pressure fuel injection using equilibrium thermodynamics. *Int. J. Multiphase Flow* **72**, 24–38.

Qiu, L., Wang, Y., Jiao, Q., Wang, H. & Reitz, R. D. 2014 Development of a thermodynamically consistent, robust and efficient phase equilibrium solver and its validations. *Fuel* **105**, 1–16.

Terashima, H. & Koshi, M. 2012 Approach for simulating gas–liquid-like flows under supercritical pressures using a high-order central differencing scheme. *J. Comput. Phys.* **231**, 6907–6923.

Wehrfritz, A., Vuorinen, V., Kaario, O. & Larmi, M. 2013 Large Eddy Simulation of High-Velocity Fuel Sprays: Studying Mesh Resolution and Breakup Model Effects for Spray A. *Atomization Spray* **23**, 419–442.

Xue, Q., Som, S., Senecal, P. K. & Pomraning, E. 2013 Large Eddy Simulation of Fuel-Spray Under Non-Reacting Ic Engine Conditions. *Atomization Spray* **23**, 925–955.